Influence of Vacancy Ordering on the Percolative Behavior of $(Li_{1-x}Na_x)_{3y}La_{2/3-y}TiO_3$ Perovskites

C. P. Herrero,[†] A. Varez,[‡] A. Rivera,[§] J. Santamaría,[§] C. León,[§] O. V'yunov,[||] A. G. Belous,[||] and J. Sanz*,[†]

Instituto Ciencia de Materiales de Madrid (CSIC), Cantoblanco, 28049 Madrid, Spain, GFMC, Departamento de Física Aplicada III, Facultad de Física, Universidad Complutense de Madrid, 28040 Madrid, Spain, Solid State Chemistry, Institute of Inorganic Chemistry, Ukrainian Academy of Sciences, 252680 Kiev, Ukraine, and Departamento Ciencia de Materiales, Universidad Carlos III, 28911 Leganés, Spain

Received: August 31, 2004; In Final Form: November 2, 2004

Influence of the vacancy concentration on the Li conductivity of the $(Li_{1-x}Na_x)_{0.2}La_{0.6}TiO_3$ and $(Li_{1-x}Na_x)_{0.5}La_{0.5}TiO_3$ perovskite series, with $0 \le x < 1$, has been investigated by neutron diffraction (ND), impedance spectroscopy (IS), nuclear magnetic resonance (NMR), and Monte Carlo simulations. In both series, Li^+ ions occupy unit cell faces, but Na^+ ions are located at A sites of the perovskite. From this fact, the amount of vacant A sites that participate in Li conductivity is given by the expression $n_v = [Li] + \square$, where $\square$ is the nominal vacancy concentration. Substitution of Li by Na decreases the amount of vacancies, reducing drastically the Li conductivity when n_v approaches the percolation threshold of the perovskite conduction network. In disordered $(Li_{1-x}Na_x)_{0.5}La_{0.5}TiO_3$ perovskites, the percolation threshold is 0.31; however, in ordered $(Li_{1-x}Na_x)_{0.2}La_{0.6}TiO_3$ perovskites, this parameter changes to 0.26. Near the percolation threshold, the amount of mobile Li species deduced by ^7Li NMR spectroscopy is lower than that derived from structural formulas but higher than deduced from dc conductivity measurements. Conductivity values have been explained by Monte Carlo simulations, which assume a random walk for Li ions in the conduction network of the perovskite. In these simulations, distribution of vacancies conforms to structural models deduced from ND experiments.

Introduction

Fast ion conductors are characterized by a disordered distribution of mobile ions in structural networks containing vacant sites that are energetically equivalent to sites occupied by mobile ions. The presence of vacant sites allows the ions to hop from site to site through the structure and eventually gives rise to a long-range ionic transport. In general, ion conductivity is proportional to the concentration of mobile ions, n_c, and to their mobility, which increases in a high number of cases with the amount of vacant sites n_v. However, a detailed description of ion conductivity must include the configurational entropy describing the vacancy distribution in the solid.

Since the discovery of high ionic conductivity in the $Li_{3y}La_{2/3-y}TiO_3$ series,[1,2] with a perovskite structure (LLTO), this system has been extensively studied to analyze structural features that improve the mobility of lithium ($\sigma_{dc} \approx 10^{-3}$ S cm^{-1} at 300 K).[3] In these perovskites, La^{3+} ions can be substituted by Li^+ ions, and the amount of nominal vacant A sites is given by $\square = {}^1/_3 - 2y$. In orthorhombic perovskites, $y < 0.06$, the ordering of vacancies in alternate planes favors the two-dimensional mobility of lithium.[3−6] In samples with higher Li contents, $y > 0.1$, the ordering of vacancies decreases and the structure becomes tetragonal.[6,7] Finally, in rhombohedral Li-rich samples quenched from high temperature,[8−10] ordering is removed and Li mobility displays a three-dimensional character.

Neutron diffraction (ND) experiments in $Li_{3y}La_{2/3-y}TiO_3$ perovskites indicated that Li ions occupy the center of square windows that connect contiguous vacant A sites.[11,12] This arrangement is the most stable configuration for lithium and underlines the role played by square window geometry in transport properties. On the other hand, the shift of lithium from A sites to unit cell faces of the perovskite causes the amount of vacant A sites that participate in Li conduction to increase with respect to that deduced from the structural formula. This fact explains that Li mobility in $Li_{0.5}La_{0.5}TiO_3$ perovskite, without nominal vacancies, is one of the highest reported in the $Li_{3y}La_{2/3-y}TiO_3$ series.[13−15]

In the $(Li_{1-x}Na_x)_{0.5}La_{0.5}TiO_3$ (LNLTO) series, the structural analysis showed that Na ions occupy A sites, while Li ions are located at the unit cell faces of the perovskite.[16] In accordance with this fact, the number of vacant A sites was reduced with the Na content, and the conductivity decreased 6 orders of magnitude when the sodium content approached 0.2 per structural formula.[16,17] This fact was interpreted on the basis of percolation theory, which assumes that the ion conductivity decreases drastically when the amount of vacant A sites in the conduction network, $n_v = [Li] + \square$, approaches the percolation threshold for a cubic lattice ($n_p = 0.31$).[18]

In this paper, structural features of orthorhombic $(Li_{1-x}Na_x)_{0.2}La_{0.6}TiO_3$ (ordered) and rhombohedral $(Li_{1-x}Na_x)_{0.5}La_{0.5}TiO_3$ (disordered) perovskites have been investigated with the Rietveld method. For this, neutron diffraction (ND) patterns of the two

* To whom correspondence should be addressed. E-mail: jsanz@icmm.csic.es. Tel: 34-913349075. Fax: 34-913720623.
[†] Instituto Ciencia de Materiales de Madrid (CSIC).
[§] Universidad Complutense de Madrid.
[||] Ukrainian Academy of Sciences.
[‡] Universidad Carlos III.

10.1021/jp046076p CCC: $30.25
Published on Web 01/22/2005

series, recorded at room temperature, have been analyzed. Concerning cation mobility, ^{7}Li NMR spectroscopy has been used to analyze the local mobility and impedance spectroscopy (IS) to determine the long-range mobility of lithium. A Monte Carlo method has been finally used to analyze the influence of vacancy distribution on the Li conductivity of these perovskites.

Experimental Section

Sample Preparation. $(Li_{1-x}Na_x)_{0.2}La_{0.6}TiO_3$ and $(Li_{1-x}Na_x)_{0.5}La_{0.5}TiO_3$ perovskites, with $0 \leq x < 1$, were synthesized from stoichiometric amounts of Li_2CO_3, Na_2CO_3, La_2O_3, and TiO_2 (high purity grade), following refs 9 and 10. To reduce the absorption cross section in neutron diffraction experiments, a ^{7}Li-enriched reagent was used. Before reaction, Li_2CO_3 and Na_2CO_3 compounds were dried at 300 °C, TiO_2 was dried at 600 °C, and La_2O_3 was dried at 700 °C. Mixtures were ground in an agate mortar with acetone and calcined in air for 12 h at 800 °C to eliminate CO_2. To avoid the loss of alkaline elements, the temperature was increased at 1 °C/min. The calcined powders were then ground, pressed into pellets under a pressure of 500 kg/cm^2 (50 MPa), and heated at 1150 °C. Finally, ground powders were pressed and heated at 1330 °C for 6 h. From this temperature, $(Li_{1-x}Na_x)_{0.2}La_{0.6}TiO_3$ samples were cooled slowly (1 °C/min) to room temperature, while samples of the $(Li_{1-x}Na_x)_{0.5}La_{0.5}TiO_3$ series were quenched into liquid nitrogen. Inductively coupled plasma spectroscopy (ICP), using a JY-70 Plus spectrometer, was used to evaluate the metal molar ratio. In all cases, chemical data conformed to nominal compositions.

Experimental Techniques. ND patterns were collected in the high-resolution powder diffractometer D1A at ILL-Grenoble. A wavelength of 1.912 Å was selected from a Ge monochromator. The counting time was 4 h, using about 4 g of sample contained in a vanadium can. In the first step, ND patterns were indexed with the Treor program. Afterwards, the Rietveld analysis of ND patterns was carried out with the Fullprof program. In structural refinements, a pseudo-Voigt function was chosen to reproduce the line shape of diffraction peaks. In this analysis, coherent scattering lengths used for La, Li, Na, Ti, and O were 8.24, −1.90, 3.63, −3.30, and 5.80 fm.

^{7}Li NMR spectra were obtained at room temperature in a MSL-400 Bruker spectrometer working at 155.45 MHz. Static and magic angle spinning (MAS) NMR spectra were taken after irradiation of the sample with a $\pi/2$ pulse (3 μs). In MAS experiments, the rotor was of Andrew type. The spinning frequencies used were selected to have a similar number of sidebands for determination of quadrupole constants; in $(Li_{1-x}Na_x)_{0.5}La_{0.5}TiO_3$ the spinning rate was 4 kHz and that in $(Li_{1-x}Na_x)_{0.2}La_{0.6}TiO_3$ was 10 kHz. The analysis of NMR spectra was carried out with the Winfit software package (Bruker).

Sintered cylindrical pellets of 13 mm diameter and 1 mm thickness, pasted with silver electrodes on both faces, were used for electrical measurements. Impedance spectroscopy measurements were conducted at room temperature in the frequency range 20 Hz−30 MHz, using HP4284A and HP4285A precision LCR meters. Measurements were carried out under a N_2 flow to ensure an inert atmosphere. From conductivity vs frequency plots, σ_{dc} values of perovskites were deduced at room temperature and analyzed as a function of the sample composition.

Monte Carlo Simulations. To understand the dependence of the ionic conductivity on the sample composition, Monte Carlo simulations of Li diffusion were undertaken in two perovskite series. Diffusion coefficients, D, are related to ionic conductivities, σ, through the expression

$$\sigma_{dc} = \frac{nq^2D}{k_BT}$$

where n and q indicate the concentration and electric charge of diffusing species. This equation can be derived from the Nernst−Einstein equation.[19] Thus, at a given temperature T, σ_{dc} is proportional to D. For computational reasons, it is easier to obtain the atomic diffusion coefficient for a stochastic process than to calculate the conductivity in the presence of an external bias voltage.

In accord with the Li conductivity measured in the $Li_{3x}La_{2/3-x}TiO_3$ series, we have assumed that Li ions move randomly in the perovskite structure, and activation energies are the same in both series.[20] In each step of the simulation Li ions are allowed to jump only to nearest-neighbor sites. These jumps are not allowed when sites A of the corresponding cells are occupied by La or Na cations. In these calculations, we have considered 100 × 100 × 100 supercells of the perovskite unit cell. Some simulations have been carried out for larger supercells to check that finite-size effects do not change our results at the precision level presented below.

In all perovskites analyzed, Li ions occupy unit cell faces of the perovskite; from this fact, the amount of vacant A sites, $n_v = [Li] + \square$, is clearly higher than deduced from the structural formula. In rhombohedral $(Li_{1-x}Na_x)_{0.5}La_{0.5}TiO_3$ samples, Na and La occupy the same crystallographic site and vacancies are randomly distributed in the perovskite.[16] In orthorhombic $(Li_{1-x}Na_x)_{0.2}La_{0.6}TiO_3$ samples, cations and vacancies are distributed on two sites, according to occupancies derived by neutron diffraction analysis. In these perovskites, fully occupied planes $z/c = 0$ alternate with planes $z/c = 0.5$, in which the amount of vacancies is higher than deduced from the structural formula.

In rhombohedral samples, diffusion coefficients were calculated as

$$D = \lim_{t\to\infty} \frac{\langle(\mathbf{r} - \mathbf{r}_0)^2\rangle}{6t}$$

where t is the diffusing time, measured in steps of the Monte Carlo procedure (number of jump attempts per Li cation). In orthorhombic perovskites, lithium diffusion is anisotropic, and diffusion coefficients must be calculated separately along three crystal directions; i.e.

$$D_i = \lim_{t\to\infty} \frac{\langle(x_i - x_{0i})^2\rangle}{2t} \quad i = 1-3$$

From calculated values, D_i, the mean value was obtained according to the expression

$$D = (D_x + D_y + D_z)/3$$

Results

ND Analysis. ND patterns of $(Li_{1-x}Na_x)_{0.5}La_{0.5}TiO_3$ and $(Li_{1-x}Na_x)_{0.2}La_{0.6}TiO_3$ series recorded at 300 K are shown in Figures 1 and 2, respectively. In all samples, ND patterns correspond to the perovskite, indicating that the amount of secondary phases is small (arrows in Figure 1). In the $(Li_{1-x}Na_x)_{0.5}La_{0.5}TiO_3$ series, ND patterns were indexed with the rhombohedral $\sqrt{2}a_p,\sqrt{2}a_p,2\sqrt{3}a_p$ unit cell ($R\bar{3}c$ space group), with parameters $a \approx 5.476$ Å and $c \approx 13.417$ Å (see Table 1). In the $(Li_{1-x}Na_x)_{0.2}La_{0.6}TiO_3$ series, the best refinement was obtained by considering an orthorhombic doubled $2a_p,2a_p,2a_p$

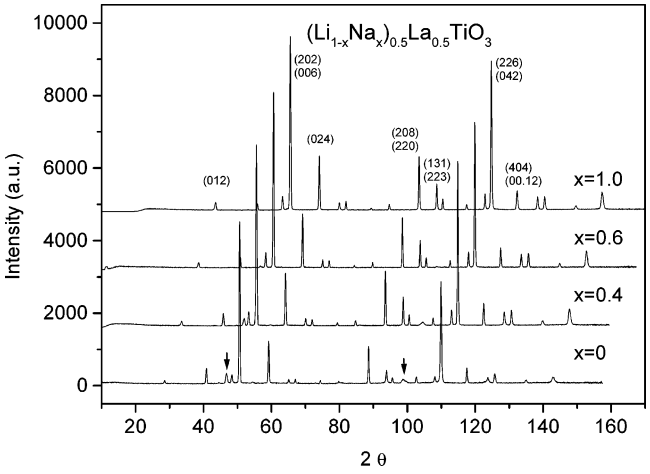

Figure 1. ND patterns of the $(Li_{1-x}Na_x)_{0.5}La_{0.5}TiO_3$ series, $x = 0$, 0.4, 0.6, 1.0, recorded at room temperature.

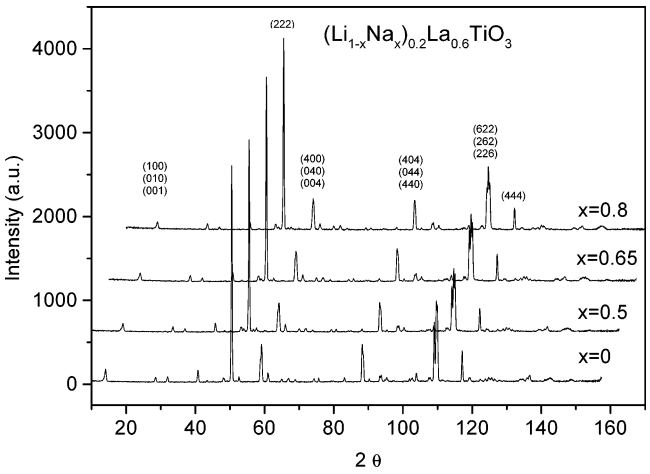

Figure 2. ND patterns of $(Li_{1-x}Na_x)_{0.2}La_{0.6}TiO_3$ series, $x = 0$, 0.5, 0.65, 0.8, recorded at room temperature.

perovskite (*Cmmm* space group), with parameters $a \approx 7.729$ Å, $b \approx 7.749$ Å, and $c \approx 7.784$ Å (see Table 2). In both series, unit cell parameters remain basically constant with composition.

Structural features of perovskites have been analyzed with the Rietveld method. In this study, rhombohedral and orthorhombic models previously reported have been used (see Table 3).[5,11] During refinements, thermal factors of La and Na atoms were constrained to vary together. In rhombohedral samples, Ti is located at the center of regular TiO_6 octahedra (Ti−O ≈ 1.943 Å). In these perovskites, the antiphase tilting of TiO_6 octahedra along the [111] direction produces an appreciable distortion of LaO_{12} cuboctahedra, in which three La−O distances were measured (2.52, 2.76, and 2.96 Å). In orthorhombic samples, Ti is shifted toward vacancy-rich planes ($z/c = 0.5$), producing two different Ti−O distances along the *c* axis (Ti−$O_1 \approx 1.87$ and Ti−$O_5 \approx 2.02$ Å) and four Ti−O distances near 1.94 Å in perpendicular planes. In these perovskites, the octahedral tilting is produced along the *b* axis, inducing again an important distortion in LaO_{12} cuboctahedra.

The analysis of the rhombohedral $(Li_{1-x}Na_x)_{0.5}La_{0.5}TiO_3$ series showed that Na and La ions occupy the same sites of the perovskite (6a Wyckoff sites) but Li ions are located at the center of unit cell faces of the ideal perovskite (18d Wyckoff sites).[11] The analysis of the orthorhombic $(Li_{1-x}Na_x)_{0.2}La_{0.6}TiO_3$ series showed the presence of two sites for La and Na in alternating planes along the *c* axis (4i and 4j Wyckoff sites). In these samples, vacancies are preferentially accumulated in $z/c = 0.5$ planes; showing that dimensions of square windows that connect contiguous A sites in these planes are appreciably larger than those of $z/c = 0$ planes. Fourier map differences calculated in $Li_{0.2}La_{0.6}TiO_3$ showed that Li ions are preferentially located at the center of unit cell faces of the perovskite, in $z/c = 0.25$ and $z/c = 0.5$ planes.[12] Substitution of Li by Na reduces in a preferential way the amount of vacancies in $z/c = 0.5$ planes (see Table 2).

NMR Spectroscopy. ^{7}Li NMR spectra of Li ions ($I = {}^3/_2$) are formed by a central ($-{}^1/_2$, ${}^1/_2$) and two satellite ($-{}^1/_2$, $-{}^3/_2$) and ($+{}^1/_2$, $+{}^3/_2$) transitions. In the ^{7}Li MAS NMR spectra of analyzed perovskites, the last transitions are modulated by the spinning sidebands produced by the rotation of the sample (Figures 3 and 4). From the analysis of spinning-sideband patterns, quadrupolar C_Q and η constants were determined.

The ^{7}Li MAS NMR spectrum of mobile species is formed by a single line; however, that of species with restricted mobility displays a quadrupole pattern. According to crystallographic data, the ^{7}Li MAS NMR spectrum of the $Li_{0.5}La_{0.5}TiO_3$ sample is formed by one narrow component but that of the $Li_{0.2}La_{0.6}TiO_3$ sample is formed by two components; one narrow component and another broader one displaying satellite transitions (bottom of Figures 3 and 4). This fact illustrates that the mobility of lithium must be important in 18d sites of rhombohedral perovskites but the mobility of lithium in 4i sites must be lower than that of 4j sites in orthorhombic perovskites. However, the relative intensity of the broader component is higher than that deduced from ND analysis, indicating that exchanging processes between two sites are produced (Figure 4). Exchange processes cause the broadening detected in spinning sidebands of ^{7}Li MAS NMR spectra.

The amount of mobile Li ions ($C_Q \approx 0$) decreases with the incorporation of sodium in the $(Li_{1-x}Na_x)_{0.5}La_{0.5}TiO_3$ series (Figure 3). The ^{7}Li MAS NMR spectrum of $Li_{0.5}La_{0.5}TiO_3$ is formed by a single narrow component ascribed to mobile species; however, that of $(Li_{1-x}Na_x)_{0.5}La_{0.5}TiO_3$ samples corresponds to two types of Li with different mobilities. The amount of fixed species increases at expenses of mobile species for $x > 0.4$ [Li] < 0.3). The ^{7}Li MAS NMR spectrum of the $Li_{0.1}Na_{0.4}La_{0.5}TiO_3$ perovskite ($x = 0.8$) was reproduced with a single spinning-sideband pattern with parameters $C_Q = 60$ kHz and $\eta = 0.5$. This pattern has been ascribed to Li ions located at oxygen square windows of the perovskite, having very low mobility. According to this fact, the line width of spinning sidebands is very low.

In the $(Li_{1-x}Na_x)_{0.2}La_{0.6}TiO_3$ series, the incorporation of sodium again reduces the amount of mobile species (Figure 4). In the $Li_{0.2}La_{0.6}TiO_3$ sample ($x = 0$), the ^{7}Li MAS NMR spectrum is formed by two Li species with different mobilities that have been ascribed to Li ions located at the $z/c = 0.25$ and $z/c = 0.5$ planes. Exchange processes between both species decrease when the Na content increases above $x = 0.5$, producing the enlargement of the spectral region occupied by spinning sidebands (increase of quadrupolar C_Q values). The line width of spinning sidebands of fixed species is again considerably reduced. The ^{7}Li MAS NMR spectrum of the $Li_{0.04}Na_{0.16}La_{0.6}TiO_3$ perovskite ($x = 0.8$) was reproduced by two components with $C_Q = 0$ kHz and $C_Q = 120$ kHz ($\eta = 0.5$). The Rietveld analysis of ND patterns showed that the amount of vacancies at $z/c = 0.5$ planes decreases when the amount of Na increases. According to this fact, the amount of Li species at $z/c = 0.25$ planes that exchange with $z/c = 0.5$ planes, deduced from NMR spectra, decreases with the Na content.

TABLE 1: Refined Structural Parameters of $(Li_{1-x}Na_x)_{0.5}La_{0.5}TiO_3$ Using the Rhombohedral Model ($R\bar{3}c$ Space Group)

x	*a*	*c*	*B*(La/Na)	*B*(Li)	*B*(Ti)	$B(O_{eq})^a$	La(occ)	Na(occ)	Li(occ)	R_I	R_F	R_p	R_{wp}	$\chi^{2\,b}$
0	5.4757(5)	13.417(2)	0.19(17)	11.8	1.15(18)	2.48	0.495		0.50	5.4	3.6	7.0	10.1	2.15
0.4	5.4783(2)	13.415(1)	0.27(9)	9.72	0.87(14)	1.41	0.519	0.198	0.30	3.8	2.8	7.5	10.4	4.42
0.6	5.4794(2)	13.414(1)	0.42(15)	9.98	0.89(18)	1.23	0.501	0.27	0.20	1.7	1.1	5.7	8.2	1.97
1.0	5.4858(1)	13.4174(6)	0.86(7)		0.76(9)	1.16	0.477	0.543	0.000	2.8	2.0	6.0	8.7	2.63

[a] $B_{eq} = {}^4/_3\{a_1a_1\beta_{11} + a_2a_2\beta_{22} + cc\beta_{33} + a_1a_2\beta_{12} + a_1c\beta_{13} + a_2c\beta_{23}\}$. [b] A total of 20 parameters were used in the refinement.

TABLE 2: Refined Structural Parameters of $(Li_{1-x}Na_x)_{0.2}La_{0.6}TiO_3$ Using the Orthorhombic Model (*Cmmm* Space Group)

x	*a*	*b*	*c*	*B*(La/Na)	*B*(Ti)	$B(O_{eq})^a$	La1(occ)	La2(occ)	Na2(occ)	R_I	R_F	R_p	R_{wp}	$\chi^{2\,b}$
0	7.7294(1)	7.7489(1)	7.7839(1)	0.60	0.55	1.11	0.97	0.25		6.4	6.7	5.0	7.1	7.6
0.5	7.7310(2	7.7567(2)	7.7909(2)	0.69	0.49	1.24	0.95	0.25	0.16	5.5	7.8	7.4	10.4	2.50
0.65	7.7288(2)	7.7561(2)	7.7884(2)	0.39	0.14	0.99	0.97	0.23	0.23	4.6	6.7	7.0	9.8	2.50
0.8	7.7282(2)	7.7554(2)	7.7840(2)	0.54	0.47	1.12	0.94	0.26	0.31	4.9	7.2	6.3	8.1	1.74

[a] Averaged thermal factor of five oxygen atoms. [b] A total of 31 parameters were used in the refinement.

TABLE 3: Positional Parameters for Rhombohedral and Orthorhombic Perovskites Used in Structural Refinements

space group $R\bar{3}c^a$			space group $Cmmm^b$		
atom	site	atomic coord	atom	site	atomic coord
La	6a	0, 0, $^1/_4$	La1	4i	0, $y \approx {}^1/_4$, 0
Li	18d	$^1/_2$, 0, 0	La2	4j	0, $y \approx {}^1/_4$, $^1/_2$
Ti	6b	0, 0, 0	Ti	8o	$x \approx {}^1/_4$, 0, $z \approx {}^1/_4$
			O1	4g	$x \approx {}^1/_4$, 0, 0
			O2	4k	0, 0, $z \approx {}^1/_4$
			O3	4l	0, $^1/_2$, $z \approx {}^1/_4$
			O4	8m	$^1/_4$,$^1/_4$, $z \approx {}^1/_4$
O	18e	$x \approx {}^1/_2$, 0, $^1/_4$	O5	4h	$x \approx {}^1/_4$, 0, $^1/_2$

[a] Taken from ref 11. [b] Taken from ref 5.

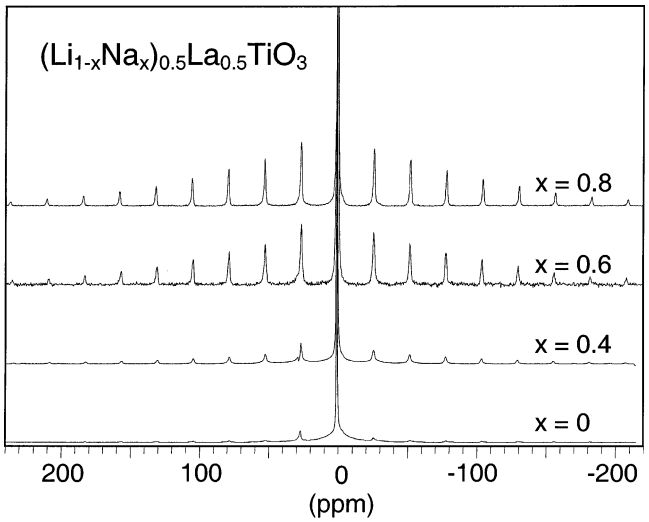

Figure 3. ^{7}Li MAS NMR spectra of the $(Li_{1-x}Na_x)_{0.5}La_{0.5}TiO_3$ series, recorded at room temperature with a spinning rate of 4 kHz.

The presence of several nonresolved components in ^{7}Li MAS NMR spectra of two series makes difficult the analysis of relaxation processes (T_1 and T_2 times).

Impedance Spectroscopy. Figure 5a shows the dependence of dc conductivity of $(Li_{1-x}Na_x)_{0.2}La_{0.6}TiO_3$ (triangles) and $(Li_{1-x}Na_x)_{0.5}La_{0.5}TiO_3$ series (diamonds) as a function of the Li content. In this figure, dc conductivity values of $Li_{3y}La_{2/3-y}TiO_3$ samples (open squares) have been included for comparison.

In rhombohedral $(Li_{1-x}Na_x)_{0.5}La_{0.5}TiO_3$ samples with [Na] < 0.2 ([Li] > 0.3), dc conductivity values are in the range of 10^{-3} S cm^{-1} at 300 K that are typical of fast ion conductors (Figure 5a). In these perovskites, a decrease of 6 orders of magnitude is observed at [Na] $= 0.2$ ([Li] ≈ 0.3). When the sodium content increases above 0.2, dc conductivity is found to decrease below the detection limit.

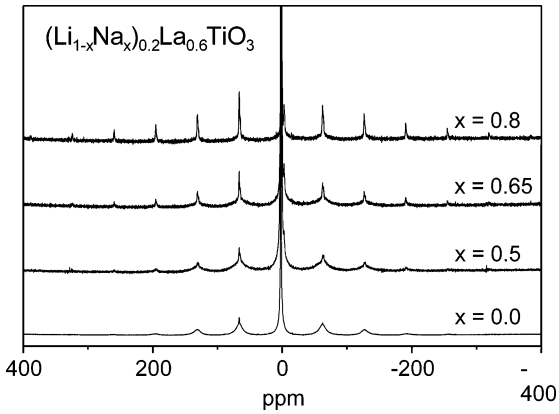

Figure 4. ^{7}Li MAS NMR spectra of the $(Li_{1-x}Na_x)_{0.2}La_{0.6}TiO_3$ series, recorded at room temperature with a spinning rate of 10 kHz.

Orthorhombic $(Li_{1-x}Na_x)_{0.2}La_{0.6}TiO_3$ samples with low sodium contents, [Na] < 0.1 ([Li] > 0.1), show values of the dc conductivity in the range of 10^{-3} S cm^{-1} at 300 K (Figure 5a). An important decrease is observed in conductivity for [Na] $=$ 0.14 ([Li] $= 0.06$). When the sodium content further increases, dc conductivity is found to be less than 10^{-10} S cm^{-1}, our experimental detection limit.

In Figure 5b, conductivity values corresponding to both series are plotted as a function of the sum of nominal vacancies plus the Li content: $n_v = [Li] + \square$. In this figure, it can be observed that the strong decrease detected in both series is produced at similar n_v values ($0.25 < n_v < 0.31$). However, a detailed analysis of conductivity values shows that the decrease observed in $(Li_{1-x}Na_x)_{0.2}La_{0.6}TiO_3$ is produced at $n_v = 0.26$, a value appreciably lower than that obtained in $(Li_{1-x}Na_x)_{0.5}La_{0.5}TiO_3$ perovskites; $n_v = 0.31$.

Monte Carlo Simulations. In Figure 6 we present diffusion coefficients, *D*, of Li ions for the two series considered here. Symbols indicate results of simulations, which are plotted in a logarithmic plot as a function of $n_v = [Li] + \square$. As shown in an earlier work, this is the relevant parameter to understand the behavior of the ionic conductivity in $(Li_{1-x}Na_x)_{0.5}La_{0.5}TiO_3$ perovskites.[16] In Figure 6, values of *D* are normalized by D_0, the diffusion coefficient corresponding to the free diffusion of ions at each temperature (no ions on A sites).

Near the percolation threshold, n_p, conductivity values deduced with the Monte Carlo method vary as $(n - n_p)^\mu$, with the exponent $\mu = 2$. This expression is typical for diffusion of atoms in three dimensions (cubic lattice).[18] In the rhombohedral series $(Li_{1-x}Na_x)_{0.5}La_{0.5}TiO_3$, a strong decrease in *D* is detected as the Li concentration approaches the percolation threshold [Li] $+ \square = 0.31$. However, in orthorhombic $(Li_{1-x}Na_x)_{0.2}La_{0.6}TiO_3$

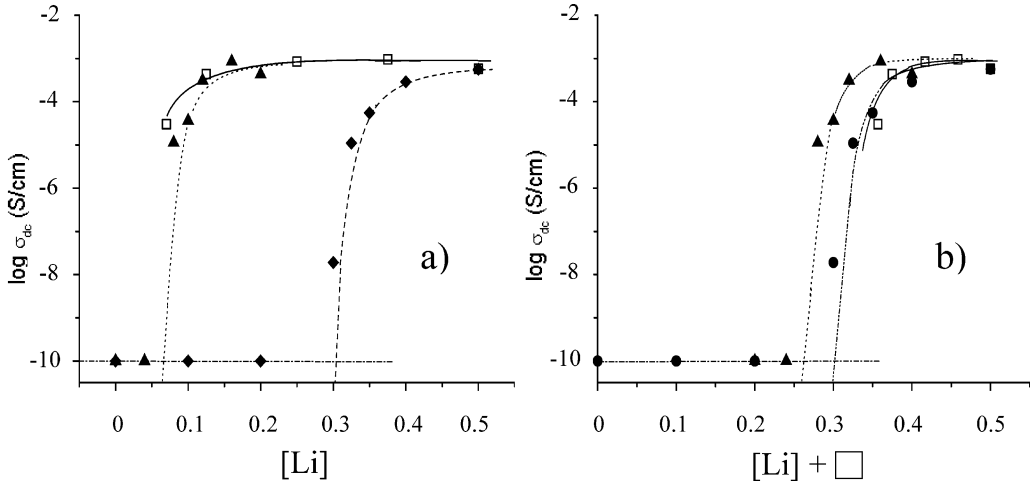

Figure 5. dc conductivity of $(Li_{1-x}Na_x)_{0.2}La_{0.6}TiO_3$ (solid triangles) and $(Li_{1-x}Na_x)_{0.5}La_{0.5}TiO_3$ (solid diamonds) samples recorded at room temperature as a function of (a) the Li content and (b) the actual vacancy concentration [Li] + □. Conductivity values of the $Li_{3y}La_{2/3-y}TiO_3$ series are included for comparison (open squares).

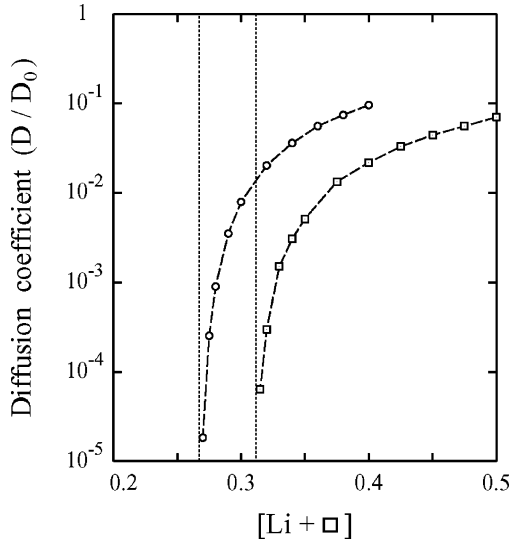

Figure 6. Normalized diffusion coefficients (D/D_0) as a function of the actual vacancy concentration [Li] + □ in $(Li_{1-x}Na_x)_{0.2}La_{0.6}TiO_3$ (circles) and $(Li_{1-x}Na_x)_{0.5}La_{0.5}TiO_3$ (squares) perovskites, as derived from Monte Carlo simulations.

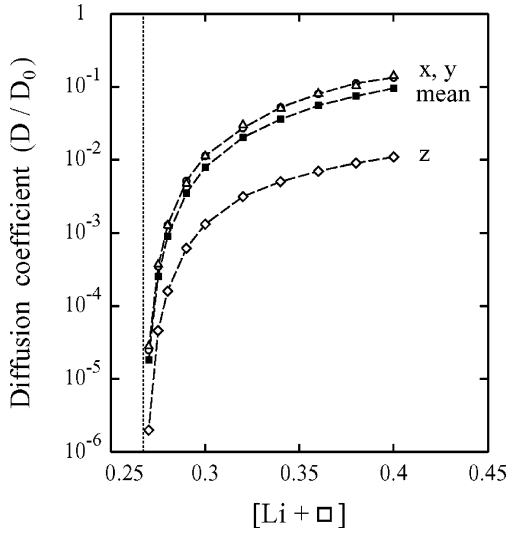

Figure 7. Dependence of diffusion coefficients, D_x/D_0, D_y/D_0 and D_z/D_0, on the actual vacancy concentration [Li] + □ in $(Li_{1-x}Na_x)_{0.2}La_{0.6}TiO_3$ perovskites.

perovskites, a similar decrease was observed for [Li] + □ = 0.26. Taking into account the nominal amount of vacancies, □ = 0 and 0.20, the percolation threshold appears at [Li] = 0.31 and 0.06, respectively, in both analyzed series.

Apart from the difference in mean diffusion coefficients of both series, another important difference is the anisotropy found for D in orthorhombic perovskites. Figure 7 shows simulation results for diffusion coefficients along the x, y, and z directions of these perovskites. As a consequence of the vacancy distribution, lithium diffusion along the z direction is always lower than in (x, y) planes, given that D_x/D_z and D_y/D_z ratios are about 10 in the whole composition range considered. An important point deduced in these calculations is that diffusion coefficients in three perpendicular directions go simultaneously to zero for [Li] + □ ≈ 0.26.

Discussion

To analyze the influence of structural features on the Li mobility of $(Li_{1-x}Na_x)_{3y}La_{2/3-y}TiO_3$ perovskites, ND patterns of ordered ($y = 0.067$) and disordered ($y = 0.167$) perovskites were analyzed with the Rietveld method. In orthorhombic $(Li_{1-x}Na_x)_{0.2}La_{0.6}TiO_3$ perovskites, distorted TiO_6 octahedra are tilted along the b axis,[5,21] but in rhombohedral $(Li_{1-x}Na_x)_{0.5}La_{0.5}TiO_3$ perovskites, regular TiO_6 octahedra are tilted along the [111] direction.[11] In both series, the octahedral tilting produces distorted LaO_{12} cuboctahedra and the rhombic distortion of square windows that connect contiguous A sites of the perovskite.[11,21]

In all analyzed perovskites, Li cations occupy the center of unit cell faces of the ideal perovskite, making the square window geometry a relevant parameter that affects Li mobility. However, the unit cell parameters and geometry of square windows do not change basically with composition in two analyzed series, suggesting that another parameter must be more relevant.

According to previous results, the location of Li ions at square windows increases the amount of vacant A sites; however, the substitution of Li by Na ions reduces the amount of vacancies. Taking into account both effects, the amount of vacant A sites that participate in ion conduction is given by n_v = [Li] + □. Results described in this work show that Li conductivity decreases when Li is substituted by Na. In the rhombohedral series $(Li_{1-x}Na_x)_{0.5}La_{0.5}TiO_3$, where the amount of vacancies is given by n_v = [Li] + □ = [Li], a strong decrease in conductivity is detected for [Li] = 0.31. Monte Carlo simulations carried

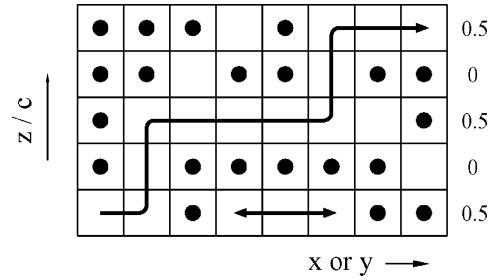

Figure 8. Schematic representation of the Li motion in ordered $(Li_{1-x}Na_x)_{0.2}La_{0.6}TiO_3$ perovskites. According to structural data, Li mobility is higher in $z/c = 0.5$ planes of the perovskite, where vacant A sites are accumulated. Li mobility along the *c* axis is produced through isolated vacant A sites of $z/c = 0$ planes.

out in this series showed that this decrease corresponds to the percolation threshold deduced for a cubic lattice. Below the percolation threshold, the long-range transport is eliminated and the mobility of Li ions is restricted to finite distances inside clusters of connected cells with vacant A sites. According to this model, two Li species with different mobility are detected near the percolation threshold in ^{7}Li NMR spectra: the narrow component corresponds to long-range diffusing species and the broadened quadrupolar pattern corresponds to Li species displaying a reduced mobility. Below the percolation threshold, Li mobility disappears and Li ions are 4-fold coordinated at unit cell faces of the perovskite.

In orthorhombic $(Li_{1-x}Na_x)_{0.2}La_{0.6}TiO_3$ perovskites, a similar behavior is found; however, in this case the percolation threshold is shifted toward lower values: $n_v = [Li] + \square = 0.26$. Taking into account that for this series the nominal concentration of vacancies is 0.2, the percolation process is produced at [Li] = 0.06 (Figures 5a and 6). On the basis of the vacancy distribution deduced from the Rietveld analysis of ND patterns, two different cases must be considered. In planes $z/c = 0$, Li diffusion should be blocked because $n_v = [Li] + \square < 0.1$ (see Table 2) is always lower than the percolation threshold corresponding to a two-dimensional diffusion ($n_p = 0.59$). However, in $z/c = 0.5$ planes where the amount of vacancies is clearly higher, Li diffusion is still possible in Li-rich members of the $(Li_{1-x}Na_x)_{0.2}La_{0.6}TiO_3$ series.

To better understand percolation processes in orthorhombic perovskites, the characteristics of Li diffusion have to be discussed. In particular, an important question is whether the ionic diffusion in orthorhombic $(Li_{1-x}Na_x)_{0.2}La_{0.6}TiO_3$ perovskites has a 2D or a 3D character. Figure 7 shows simulated diffusion coefficients along the crystallographic axes *x*, *y*, and *z*. As a consequence of the vacancy ordering, deduced by Rietveld analysis of ND patterns, lithium diffusion along the *z* direction is lower than in (*x*, *y*) planes. This result agrees with conductivity data measured in a monocrystalline sample, which showed that conductivity along the *c* axis was slightly lower than that measured along the (*x*, *y*) plane.[22] However, it is important to note that diffusion coefficients along the three axes go simultaneously to zero when [Li] + □ approaches 0.26, which indicates that diffusion cannot be strictly two-dimensional.

For [Li] + □ slightly larger than 0.26, $z/c = 0.5$ planes still contain enough free sites to allow a considerable mobility of lithium in vacancy-rich domains. The existence of a small amount of vacant A sites in $z/c = 0$ planes only permits ionic diffusion through them, giving a nonvanishing diffusion along the *z* direction. In this case, Li ions pass to adjacent $z/c = 0.5$ planes, favoring the long-range diffusion in (*x*, *y*) planes (Figure 8). According to Monte Carlo simulations, the long-range diffusion along the *x*, *y*, and *z* directions is only eliminated when [Li] + □ approaches 0.26. According to NMR data, the amount of mobile species that exchange their positions between $z/c = 0.25$ and 0.5 planes decreases considerably when the amount of vacancies approaches the percolation threshold $n_p \approx 0.26$ ($x = 0.7$). In accord with this fact, two species have been detected in ^{7}Li NMR spectra of orthorhombic perovskites, which correspond to Li ions diffusing inside vacant-rich domains of planes $z/c = 0.5$ (central narrow component) and to Li ions exchanging their positions between $z/c = 0.25$ and 0.5 planes (broadened quadrupolar pattern). Below the percolation threshold, the amount of exchanging species decreases considerably and ^{7}Li MAS NMR spectra are formed by fixed Li ions at $z/c = 0.25$ and Li species displaying local mobility in vacant rich domains in $z/c = 0.5$ planes. In accord with this fact, long-range diffusion of Li species is completely blocked along three axes in samples with $x > 0.7$.

In the case of $Li_{3y}La_{2/3-y}TiO_3$ samples, the amount of vacancies $n_v = [Li] + \square$ increases from 0.33 to 0.5 when *y* increases from 0 to 0.16. From this fact, we can see that conductivity is not considerably affected by percolation processes in this series (open squares of Figure 5). This explains why the amount of mobile species detected in ^{7}Li NMR spectra is always very high. The results described in this work differ considerably from those based on the $n_c n_v$ dependence of the conductivity. If [Li] and □ are given by the expressions $3y$ and $^1/_3 - 2y$, conductivity values should display a maximum at intermediate compositions ([Li] ≈ 0.25). This prediction has not been confirmed experimentally in $Li_{3y}La_{2/3-y}TiO_3$ perovskites.[13,14]

From the results described in this work, it can be concluded that Li mobility is similar in all perovskites placed above the percolation threshold. Taking into account that vacant sites are energetically equivalent to sites occupied by lithium, the relevant variable to understand ionic conductivity is the amount of vacancies defined by the expression $n_v = [Li] + \square$. When the amount of vacancies decreases below the percolation threshold, conductivity decreases drastically below the detection limit. On the other hand, the percolation threshold depends on the nature and distribution of alkaline cations. In $Li_{3y}La_{2/3-y}TiO_3$ perovskites, an interconnected pathway for the Li diffusion is always produced. In $(Li_{1-x}Na_x)_{3y}La_{2/3-y}TiO_3$ perovskites, the Rietveld analysis of ND patterns of $(Li_{1-x}Na_x)_{0.5}La_{0.5}TiO_3$ series showed that vacancies are disordered, but in the $(Li_{1-x}Na_x)_{0.2}La_{0.6}TiO_3$ series vacancies are preferentially accumulated in $z/c = 0.5$ planes. Monte Carlo simulations have shown that vacancy ordering is the cause of the decrease observed in the percolation threshold of orthorhombic perovskites.

Conclusions

The structure of $(Li_{1-x}Na_x)_{3y}La_{0.66-y}TiO_3$ perovskites, with $0 < x < 1$ and $y = 0.06$ or 0.16, has been deduced from the refinement of ND patterns with the Rietveld method. In orthorhombic perovskites, vacancies are ordered in alternate planes along the *c* axis; however, in rhombohedral perovskites vacancies are completely disordered. Concerning cation mobility, ^{7}Li NMR and impedance spectroscopy have been used to analyze lithium mobility. In both analyzed series, the amount of mobile species detected with NMR spectroscopy decreases progressively with the Na content; however, the conductivity decreases dramatically when the amount of vacancies, given by $n_v = [Li] + \square$, approaches the percolation threshold of the perovskite.

A Monte Carlo method has been used to analyze the influence of vacancy distribution on Li diffusion. This analysis has shown

that Li mobility is basically three-dimensional in all perovskites analyzed. In disordered $(Li_{1-x}Na_x)_{0.5}La_{0.5}TiO_3$ perovskites, the percolation threshold is $n_p = 0.31$; however, in ordered $(Li_{1-x}Na_x)_{0.2}La_{0.6}TiO_3$ perovskites, the percolation threshold decreases to 0.26. The accumulation of vacancies in $z/c = 0.5$ planes shows that a higher amount of sodium is required to block Li conductivity in ordered perovskites.

Acknowledgment. We thank the ILL for the provision of neutron beam time and the Spanish Agency CICYT (BFM-2003-03372-C03-03 and MAT-2004-03070-C05-02 projects) for financial support.

References and Notes

(1) Belous, A. G.; Novitskaya, G. N.; Polyanetskaya, S. V.; Gornikov, Y. I. *Zh. Neorg. Khim.* **1987**, *32*, 283−286.

(2) Inaguma, Y.; Chen, L.; Itoh, M.; Nakamura, T.; Uchida, T.; Ikuta, H.; Wakihara, M. *Solid State Commun.* **1993**, *86*, 689−693.

(3) Stramare, S.; Thangadurai, V.; Weppner, W. *Chem. Mater.* **2003**, *15*, 3974−3990.

(4) Paris, M. A.; Sanz, J.; Leon, C.; Santamaría, J.; Ibarra, J.; Varez, A. *Chem. Mater.* **2000**, *12*, 1694−1701.

(5) Inaguma, Y.; Katsumata, T.; Itoh, M.; Morii, Y. *J. Solid State Chem.* **2002**, *166*, 67−72.

(6) Ruiz, A. I.; López, M. L.; Veiga, M. L.; Pico, C. *Solid State Ionics* **1998**, *112*, 291−297.

(7) Bohnke, O.; Bohnke, C.; Fourquet, J. L. *Solid State Ionics* **1996**, *91*, 21−31.

(8) Harada, Y.; Hirakoso, Y.; Kawai, H.; Kuwano, J. *Solid State Ionics* **1999**, *121*, 245−251.

(9) Ibarra, J.; Várez, A.; León, C.; Santamaría, J.; Torres-Martinez, L. M.; Sanz, J. *Solid State Ionics* **2000**, *134*, 219−228.

(10) Várez, A.; Ibarra, J.; Rivera, A.; León, C.; Santamaría, J.; Laguna, M. A.; Sanjuán, M. L.; Sanz, J. *Chem. Mater.* **2003**, *15*, 225−232.

(11) Alonso, J. A.; Sanz, J.; Santamaría, J.; León, C.; Várez, A.; Fernandez-Diaz, M. T. *Angew. Chem., Int. Ed.* **2000**, *3*, 619−621.

(12) Várez, A.; Inaguma, Y.; Fernández-Díaz, M. T.; Alonso, J. A.; Sanz, J. *Chem. Mater.* **2003**, *15*(24), 4637−4641.

(13) Inaguma, Y.; Chen, L.; Itoh, M.; Nakamura, T. *Solid State Ionics* **1994**, *70*−*71*, 196−202.

(14) Kawai, H.; Kuwano, J. *J. Electrochem. Soc.* **1994**, *141*, L78−L79.

(15) León, C.; Lucía, M. L.; Santamaría, J.; París, M. A.; Sanz, J.; Varez, A. *Phys. Rev. B* **1996**, *54*, 184−189. León, C.; Santamaría, J.; París, M. A.; Sanz, J.; Ibarra, J.; Torres, L. M. *Phys. Rev. B* **1997**, *56*, 5302−5305.

(16) Rivera, A.; León, C.; Santamaría, J.; Varez, A.; V'yunov, O.; Belous, A. G.; Alonso, J. A.; Sanz, J. *Chem. Mater.* **2002**, *14*, 5148−5152.

(17) Inaguma, Y.; Itoh, M. *Solid State Ionics* **1996**, *86*−*88*, 257−260.

(18) Stauffer, D.; Aharony, A. *Introduction to Percolation Theory*; Taylor and Francis: London, 1992.

(19) Burns, G. *Solid State Physics*; Academic Press: Orlando, FL, 1985.

(20) Rivera, A.; León, C.; Santamaría, J.; Varez, A.; París, M. A.; Sanz, J. *J. Non-Cryst. Solids* **2002**, *307*−*310*, 992−998.

(21) Sanz, J.; Alonso, J. A.; Varez, A.; Fernández-Díaz, M. T. *Dalton* **2002**, 1406−1408.

(22) Inaguma, Y.; Yu, J. D.; Katsumata, T.; Itoh, M. *J. Ceram. Soc. Jpn.: Int. Ed.* **1997**, *105*(6), 548−550.